DOT/FAA/AR-01/7

Office of Aviation Research
Washington, D.C. 20591

Stress Analysis of In-Plane, Shear-Loaded, Adhesively Bonded Composite Joints and Assemblies

April 2001

Final Report

U.S. Department of Transportation
Federal Aviation Administration

NOTICE

This report is available at the Federal Aviation Administration William J. Hughes Technical Center's Full-Text Technical Reports page: actlibrary.tc.faa.gov in Adobe Acrobat portable document format (PDF).

Technical Report Documentation Page

1. Report No.	2. Government Accession No.	3. Recipient's Catalog No.
DOT/FAA/AR-01/7		

4. Title and Subtitle	5. Report Date
STRESS ANALYSIS OF IN-PLANE, SHEAR-LOADED, ADHESIVELY BONDED COMPOSITE JOINTS AND ASSEMBLIES	April 2001
	6. Performing Organization Code
7. Author(s)	8. Performing Organization Report No.
Hyonny Kim and Keith Kedward	
9. Performing Organization Name and Address	10. Work Unit No. (TRAIS)
University of California Santa Barbara Department of Mechanical & Environmental Engineering Santa Barbara, CA 93106	11. Contract or Grant No.
12. Sponsoring Agency Name and Address	13. Type of Report and Period Covered
U.S. Department of Transportation Federal Aviation Administration Office of Aviation Research Washington, DC 20591	Final Report
	14. Sponsoring Agency Code ACE-100

15. Supplementary Notes

The FAA William J. Hughes Technical Monitor was Peter Shyprykevich

16. Abstract

Recent small aircraft that have been certified in the United States, such as the Cirrus SR20 and the Lancair Columbia 300, share similar structural attributes. Specifically, they are both of nearly all-composite construction and both make extensive use of adhesive bonding as a primary method for forming structural joints. Adhesive bonding has potential for being a simple and cost-effective means by which large built-up structures can be assembled. Challenges to bonding exist in the areas regarding adhesive selection, proper surface preparation, and technician training as well as intelligent design and confidence in analyses. This report addresses the latter challenge by presenting an analysis methodology that can be used in the design of joints loaded in both tension and in-plane shear. Example calculations and applications to real structures are provided.

A closed-form stress analysis of an adhesive-bonded lap joint subjected to spatially varying in-plane shear loading is presented. The solution, while similar to Volkersen's treatment of tension-loaded lap joints, is inherently two-dimensional and, in general, predicts a multicomponent adhesive shear stress state. Finite difference and finite element numerical calculations are used to verify the accuracy of the closed-form solution for a joint of semi-infinite geometry. The stress analysis of a finite-sized doubler is also presented. This analysis predicts the adhesive stresses at the doubler boundaries and can be performed independently from the complex stress state that would exist due to a patched crack or hole located within the interior of the doubler.

When shear and tension loads are simultaneously applied to a joint, the results of stress analyses treating each loading case separately are superimposed to calculate a combined biaxial shear stress state in the adhesive. Predicting the elastic limit of the joint is then accomplished by using the von Mises yield criterion. This approach allows the calculation of a limit load envelope that maps the range of combined loading conditions within which the joint is expected to behave elastically.

This generalized analysis, while approximate, due to the nature of assumptions made in formulating the theoretical description of an in-plane, shear-loaded joint, has been shown to be accurate by alternate numerical analyses. Such analytical tools are advantageous over numerical-based solution techniques due to their mechanics-based foundation which permits the rapid exploration of parameters that can affect joint performance. This feature is especially usefulness during the design stage of an aircraft.

17. Key Words	18. Distribution Statement
Adhesive joining, In-plane shear load, Combined load, Doubler, Crack patch, General aviation	This document is available to the public through the National Technical Information Service (NTIS), Springfield, Virginia 22161.

19. Security Classif. (of this report)	20. Security Classif. (of this page)	21. No. of Pages	22. Price
Unclassified	Unclassified	36	

ACKNOWLEDGEMENTS

Deserved acknowledgement is to be given to Larry Ilcewicz and the late Donald Oplinger of the Federal Aviation Administration, John Tomblin of Wichita State University, Dieter Koehler and Todd Bevan of Lancair, and Paul Brey of Cirrus for their assistance, guidance, and funding which made this research possible.

TABLE OF CONTENTS

LIST OF FIGURES

LIST OF TABLES

EXECUTIVE SUMMARY

Recent small aircraft that have been certified in the United States, such as the Cirrus SR20 and the Lancair Columbia 300, share similar structural attributes. Specifically, they are both of nearly all-composite construction and both make extensive use of adhesive bonding as a primary method for forming structural joints. Adhesive bonding has potential for being a simple and cost-effective means by which large built-up structures can be assembled. Challenges to bonding exist in the areas regarding proper adhesive selection, surface preparation, and technician training as well as intelligent design and confidence in analyses. This report addresses the latter challenge by presenting an analysis methodology that can be used in the design of joints loaded in both tension and in-plane shear. Example calculations and applications to real structures are provided.

A closed-form stress analysis of an adhesive bonded lap joint subjected to spatially varying in-plane shear loading is presented. The solution, while similar to Volkersen's treatment of tension-loaded lap joints, is inherently two-dimensional and, in general, predicts a multicomponent adhesive shear stress state. Finite difference and finite element numerical calculations are used to verify the accuracy of the closed-form solution for a joint of semi-infinite geometry. The stress analysis of a finite-sized doubler is also presented. This analysis predicts the adhesive stresses at the doubler boundaries. It is unaffected by the stress conditions in the interior of the patch and can be performed independently from the complex stress state that would exist due to a patched crack or hole located within the interior of the doubler.

When shear and tension loads are simultaneously applied to a joint, the results of stress analyses treating each loading case separately are superimposed to calculate a combined biaxial shear stress state in the adhesive. Predicting the elastic limit of the joint is then accomplished by using the von Mises yield criterion. This approach allows the calculation of a limit load envelope that maps the range of combined loading conditions within which the joint is expected to behave elastically.

This generalized analysis, while approximate due to the nature of assumptions made in formulating the theoretical description of an in-plane, shear-loaded joint, has been shown to be accurate by alternate numerical analyses. Such analytical tools are advantageous over numerical solution techniques due to their mechanics-based foundation which permits the rapid exploration of parameters that can affect joint performance. This feature is especially useful during the design stage of an aircraft.

1. INTRODUCTION.

Recent small aircraft that have been certified in the United States, such as the Cirrus SR20 and the Lancair Columbia 300, share similar structural attributes. Specifically, they are both of nearly all-composite construction and both make extensive use of adhesive bonding as a primary method for forming structural joints. Adhesive bonding has potential for being a simple and cost-effective means by which large built-up structures can be assembled. Challenges to bonding exist in the areas regarding adhesive selection, proper surface preparation, and technician training as well as proper design and confidence in analysis. This report addresses the latter challenge by presenting an analysis methodology that can be used in the design of joints loaded in both tension and in-plane shear.

Significant attention has been directed towards the design, analysis, and testing of adhesively bonded lap joints loaded in tension [1-7]. While this mode of loading has numerous applications, many cases also exist where the lap joint is loaded by in-plane shearing forces. Examples of in-plane shear force transfer across bonded joints can be found in torsion-loaded, thin-walled structures having circumferentially and longitudinally oriented lap joints, illustrated in figure 1. Structures falling under the scope of this example are a bonded driveshaft end-fitting (circumferential joint, treated by Adams and Peppiatt [8]) and a large transport aircraft fuselage barrel built in two longitudinal halves and subsequently bonded together (longitudinal joint). An example of a small aircraft fuselage splice joint is shown in figure 2. When these structures carry torque loads, shear flow that is produced in the wall is transferred across the joint. Another example is a bonded composite shear web, shown in figure 3, typically found as an integral component in the design of aircraft wing spars. In this example, bending and torsion loads carried by the wing produce shear flow in the shear webs. For the generic configuration, shown in figure 3, load is introduced into the web through the bonded angle clips that form the structural tie between the shear web and the spar cap (or load-bearing wing skin). Sizing the geometry of this joint is dependent upon an understanding of what components of internal forces are transmitted through the joint (i.e., in-plane shear dominates), as well as an understanding of the mechanisms by which in-plane shear load is transferred across the adhesive layer from one adherend to the next.

A mechanics-based analysis of an in-plane shear-loaded bonded lap joint is presented. This analysis, derived in more detail in work by Kim and Kedward [9], treats the in-plane shear- and tension-loaded cases as uncoupled from each other. For simultaneous shear and tension loading, a multicomponent shear stress state in the adhesive is predicted by superimposing the two solutions. The resulting solution form for shear transfer is analogous to the tension-loaded lap joint case, the basic derivation of which is attributed to Volkersen [1].

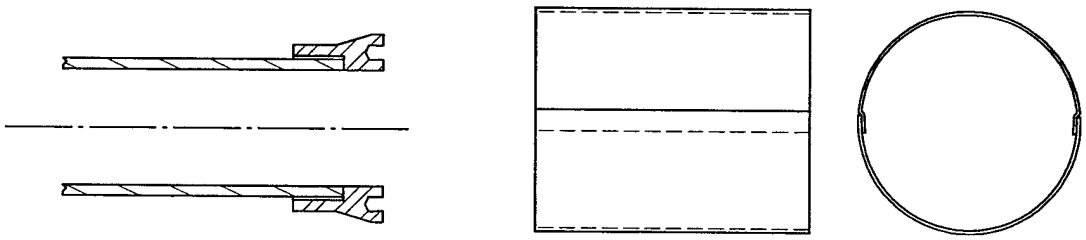

(a) Driveshaft End Fitting

(b) Longitudinal Joint

FIGURE 1. CIRCUMFERENTIAL- AND LONGITUDINAL-BONDED JOINTS

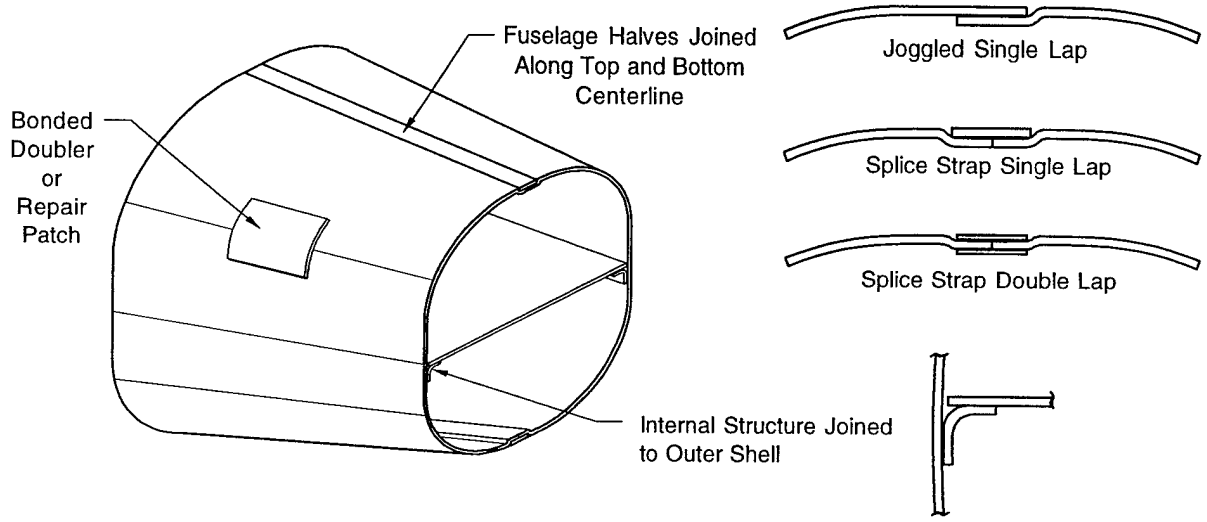

FIGURE 2. TYPICAL AFT SECTION OF SMALL AIRCRAFT BONDED FUSELAGE

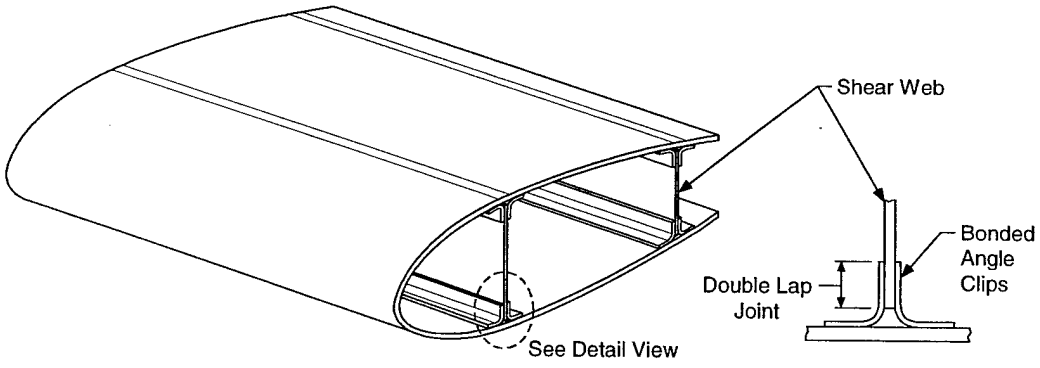

FIGURE 3. GENERIC-BONDED WING SPAR CONSTRUCTION

2. DERIVATION OF GOVERNING EQUATION.

Consider the shear-loaded, bonded lap joint shown in figure 4. The differential element in figure 4 shows the in-plane shear stresses acting on the inner and outer adherends, τ^i_{xy} and τ^o_{xy}, as well as two components of adhesive shear stress, τ^a_{xz} and τ^a_{yz}. This analysis is applicable to both the single- and double-lap joint geometries which are illustrated in figure 5. The double-lap case is limited to the condition of geometric and material symmetry about the center of the inner adherend, so that the problem is then conceptually identical to the single lap case. Alternatively, if both outer adherends have equivalent stiffness, i.e., same product of shear modulus and thickness, then the double-lap joint can still be treated as symmetric. The following conditions have been assumed:

- Constant bond and adherend thickness
- Uniform shear strain through the adhesive thickness
- Adherends carry only in-plane stresses
- Adhesive carries only out-of-plane shear stresses
- Linear elastic material behavior

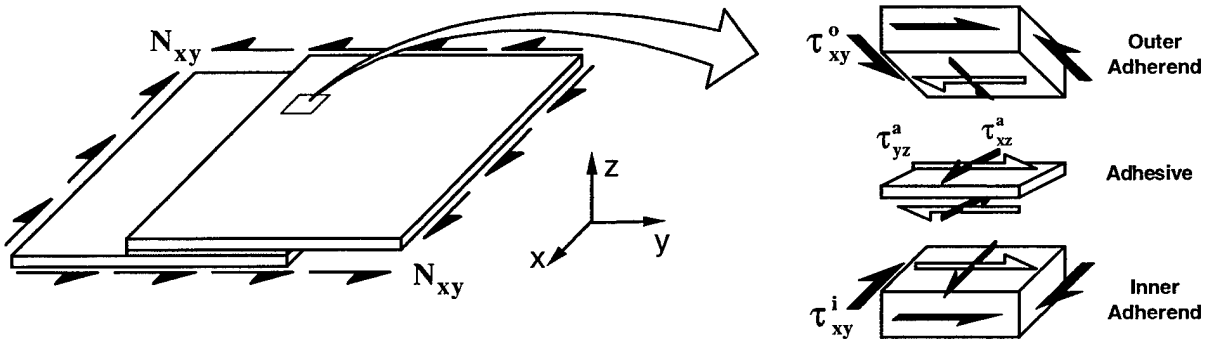

FIGURE 4. LAP JOINT TRANSFERRING SHEAR STRESS RESULTANT N_{xy} AND DIFFERENTIAL ELEMENT SHOWING ADHEREND AND ADHESIVE STRESSES

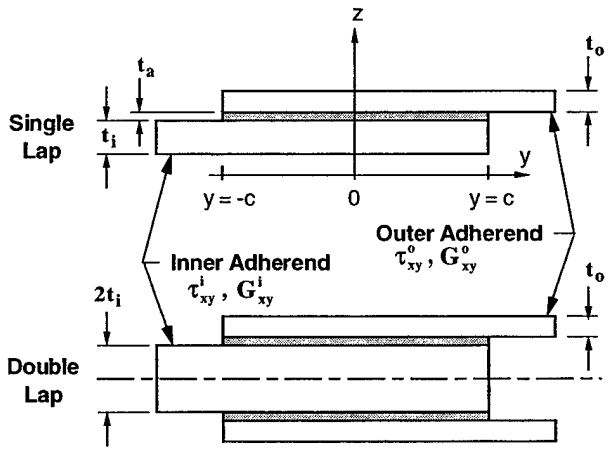

FIGURE 5. SINGLE- AND DOUBLE-LAP GEOMETRY

In figure 4, the applied shear stress resultant N_{xy} is continuous through the overlap region and, at any point, must equal the sum of the product of each adherend shear stress with its respective thickness.

$$N_{xy} = \tau_{xy}^{i} t_i + \tau_{xy}^{o} t_o \tag{1}$$

where t_i and t_o are the thickness of the inner and outer adherends, respectively, as indicated in figure 5. Force equilibrium performed on a differential element of the outer adherend, shown in figure 6, results in relationships between the adhesive stress components and the outer adherend shear stress.

$$\tau_{xz}^{a} = t_o \frac{\partial \tau_{xy}^{o}}{\partial y} \tag{2}$$

and

$$\tau_{yz}^{a} = t_o \frac{\partial \tau_{xy}^{o}}{\partial x} \tag{3}$$

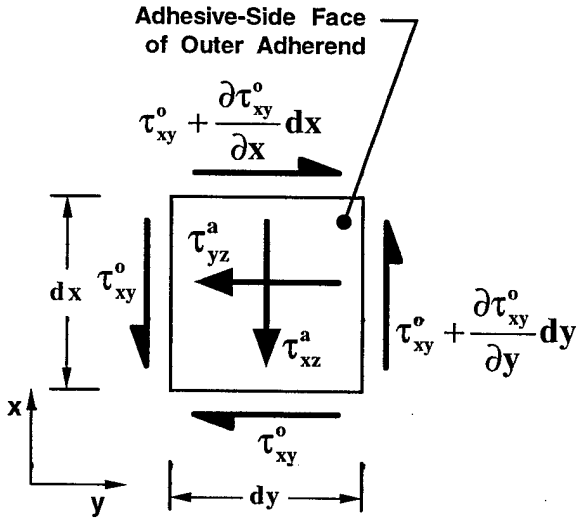

FIGURE 6. ADHESIVE AND ADHEREND STRESSES ACTING ON ELEMENT OF OUTER ADHEREND

The adhesive shear strains are written based on the assumption of uniform shear strain through the thickness of the adhesive,

$$\gamma_{xz}^{a} = \frac{\tau_{xz}^{a}}{G_a} = \frac{1}{t_a}(u_o - u_i) \tag{4}$$

and

$$\gamma_{yz}^{a} = \frac{\tau_{yz}^{a}}{G_a} = \frac{1}{t_a}(v_o - v_i) \tag{5}$$

where G_a is the adhesive shear modulus, t_a is the adhesive thickness, u_o and u_i are the outer and inner adherend displacements in the x direction, and v_o and v_i are the displacements in the y direction. Summing the y derivative of γ^a_{xz} with the x derivative of γ^a_{yz}, and combining the resulting expression with equations 1 to 3, produces a partial differential equation governing the shear stress in the outer adherend.

$$\nabla^2\tau^o_{xy} - \lambda^2\tau^o_{xy} + C_o = 0 \tag{6}$$

with

$$\lambda^2 = \frac{G_a}{t_a}\left(\frac{1}{G^o_{xy}t_o} + \frac{1}{G^i_{xy}t_i}\right) \tag{7}$$

and

$$C_o = \frac{G_a N_{xy}}{G^i_{xy}t_a t_i t_o} \tag{8}$$

This equation is generally applicable for two-dimensional problems. In equations 7 and 8, G^i_{xy} and G^o_{xy} are the in-plane shear moduli of the inner and outer adherends.

3. SOLUTION FOR SEMI-INFINITE CASE.

3.1 IN-PLANE SHEAR LOADING.

A semi-infinite joint loaded by in-plane shear is shown in figure 7. Problems can be treated using the semi-infinite assumption if load intensity drops off at the terminations of the joint, or just to size the joint at regions located away from complex boundary conditions.

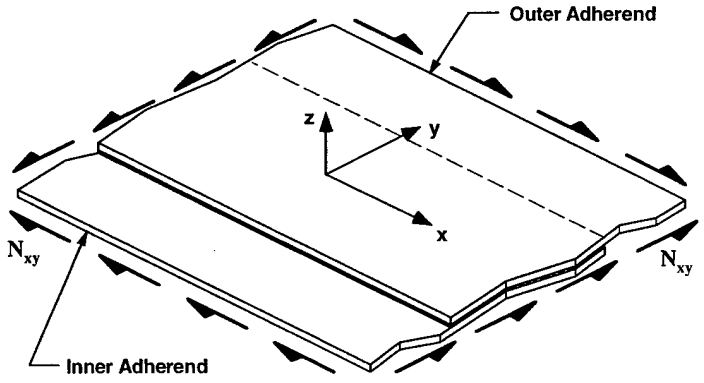

FIGURE 7. SEMI-INFINITE LAP JOINT

The adhesive shear stress components τ^a_{xz} and τ^a_{yz} can be obtained using the relationships given by equations 2 and 3, once equation 6 for τ^o_{xy} is solved. A simplifying assumption of N_{xy} being

independent of y (can be smoothly varying in x [9]) is now applied that permits a solution for the lap joint geometry shown in figure 7.

$$\tau_{xy}^{o} = A_o \cosh \lambda y + B_o \sinh \lambda y + \frac{C_o}{\lambda^2} \tag{9}$$

where λ^2 and C_o are given by equations 7 and 8. This solution satisfies the governing equation 6 exactly and is the same as that given by previous authors [10 and 11] for this simple case. Using the following boundary conditions (see joint geometry in figure 5),

$$\tau_{xy}^{o} = 0 \text{ at } y = -c \tag{10}$$

and

$$\tau_{xy}^{o} = \frac{N_{xy}}{t_o} \text{ at } y = c \tag{11}$$

the unknown terms can be determined.

$$A_o = \frac{1}{\cosh \lambda c}\left(\frac{N_{xy}}{2t_o} - \frac{C_o}{\lambda^2}\right) \tag{12}$$

and

$$B_o = \frac{N_{xy}}{2t_o \sinh \lambda c} \tag{13}$$

Substituting A_o and B_o into equation 9 gives the profile of in-plane shear stress acting in the outer adherend. The in-plane shear stress acting in the inner adherend can then be calculated using equation 1. Equation 2 is used together with equation 9 to compute the out-of-plane shear stress acting in the adhesive.

$$\tau_{xz}^{a} = t_o \frac{\partial \tau_{xy}^{o}}{\partial y} = \lambda\left[\left(\frac{N_{xy}}{2} - \frac{C_o}{\lambda^2} t_o\right)\frac{\sinh \lambda y}{\cosh \lambda c} + \frac{N_{xy}}{2}\frac{\cosh \lambda y}{\sinh \lambda c}\right] \tag{14}$$

For a joint with uniformly applied shear flow, N_{xy}, the τ_{yz}^{a} shear stress component is zero. The maximum values of adhesive shear stress occur at the ends of the bonded lap region, at $y = \pm c$. These peaks are expressed in a normalized form as

$$\frac{\left(\tau_{xz}^{a}\right)_{y=\pm c}}{\left(\tau_{xz}^{a}\right)_{ave}} = c\lambda\left[\pm\left(1 - \frac{2}{K+1}\right)\tanh \lambda c + \frac{1}{\tanh \lambda c}\right] \tag{15}$$

with

$$\left(\tau_{xz}^{a}\right)_{ave} = \frac{N_{xy}}{2c} \tag{16}$$

and

$$K = \frac{G^i_{xy} t_i}{G^o_{xy} t_o} \tag{17}$$

The peaks in adhesive shear stress are generally several times greater than the average adhesive shear stress. Note that for the case when the inner and outer adherends have the same in-plane shear stiffness, i.e., $G^i_{xy} t_i = G^o_{xy} t_o$, the term K is unity and equation 15 simplifies to

$$\frac{\left(\tau^a_{xz}\right)^{K=1}_{y=\pm c}}{\left(\tau^a_{xz}\right)_{ave}} = \frac{c\lambda}{tanh\,\lambda c} \tag{18}$$

The case of the inner and outer adherends having the same stiffness is referred to as a balanced joint.

The solution given by equation 14 is also applicable to the case when N_{xy} is a smoothly varying function of the x direction. In this case, a τ^a_{yz} stress component would exist, as indicated by equation 3, however, this stress will be small in magnitude when compared with τ^a_{xz}, even for high gradients of N_{xy} in the x direction. A detailed discussion and calculations supporting this statement are given by Kim and Kedward [9].

3.2 TENSION LOADING.

The stresses for a bonded joint loaded by tension applied in the y direction has been worked out [1, 4, and 5] and is simply provided here without derivation.

$$\tau^a_{yz} = t_o \frac{\partial \sigma^o_y}{\partial y} = \lambda_T \left[\left(\frac{N_y}{2} - \frac{C_1}{\lambda_T^2} t_o \right) \frac{sinh\,\lambda_T y}{cosh\,\lambda_T c} + \frac{N_y}{2} \frac{cosh\,\lambda_T y}{sinh\,\lambda_T c} \right] \tag{19}$$

where σ^o_y is the tensile (or compressive) stress acting in the y direction, due to an applied loading N_y. The terms λ_T and C_1 are given by

$$\lambda_T^2 = \frac{G_a}{t_a} \left(\frac{1}{E^o_y t_o} + \frac{1}{E^i_y t_i} \right) \tag{20}$$

and

$$C_1 = \frac{G_a N_y}{E^i_y t_a t_i t_o} \tag{21}$$

E^i_y and E^o_y are the respective inner and outer adherend elastic moduli in the y direction. It is clear by comparison of equation 14 with equation 19 that the solution derived for shear transfer

is analogous to the tension case. However, the chief difference lies in the governing equation 6, which is applicable for cases where the loading N_{xy} is not constant with respect to x and y, and for assemblies such as a bonded doubler reinforcement, for which the simple solution, equation 9, is not applicable.

For a balanced tension-loaded joint (i.e., $K_T = E_y^i t_i / E_y^o t_o = 1$), the normalized peak adhesive shear stress at the ends of the bond overlap is

$$\frac{\left(\tau_{yz}^a\right)_{y=\pm c}^{K_T=1}}{\left(\tau_{yz}^a\right)_{ave}} = \frac{c\lambda_T}{tanh\,\lambda_T c} \tag{22}$$

with

$$\left(\tau_{yz}^a\right)_{ave} = \frac{N_y}{2c} \tag{23}$$

3.3 COMBINED LOADING.

Figure 8 illustrates the generic profiles and directions of the shear stress acting in the adhesive for shear and tension loading. Under combined loading conditions, a multiaxial shear stress state would exist. This multiaxial stress state must be considered when predicting the joint's elastic limit and ultimate failure loads. Note that the adhesive stresses, due to in-plane shear and tension, act in directions perpendicular to each other, and thus cannot simply be summed together in order to evaluate adhesive failure. A multicomponent stress failure criterion must be used, such as the Von Mises failure criterion, for predicting the elastic limit in isotropic materials.

$$\left[\left(\tau_{xz}^a\right)^2 + \left(\tau_{yz}^a\right)^2\right]^{\frac{1}{2}} = \tau^y \tag{24}$$

where τ^y is the adhesive shear yield stress.

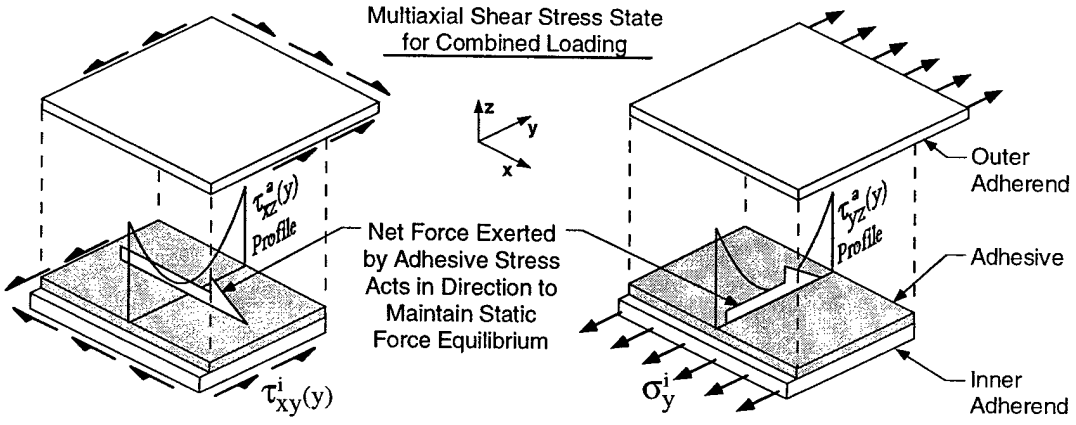

FIGURE 8. MECHANICS OF TENSION AND SHEAR LOAD TRANSFER THROUGH BONDED JOINT

3.4 EXAMPLE CALCULATIONS.

3.4.1 Glass/Epoxy and Carbon/Epoxy Joint Under Gradient Loading.

The closed-form solution developed for a semi-infinite joint is now demonstrated for the example of a bonded I-beam shear web, as illustrated in figure 9. A particular interest exists to test the solution for a shear load $N_{xy}(x)$ that is arbitrary and smoothly varying (i.e., not a linear function of x). To this end, a shear-loading function is chosen to represent the transition in shear flow in the web in the region adjacent to an applied point load, as shown in figure 9.

$$N_{xy} = 4.38\left(cos\frac{\pi x}{a} + 3\right) \text{ N/mm} \tag{25}$$

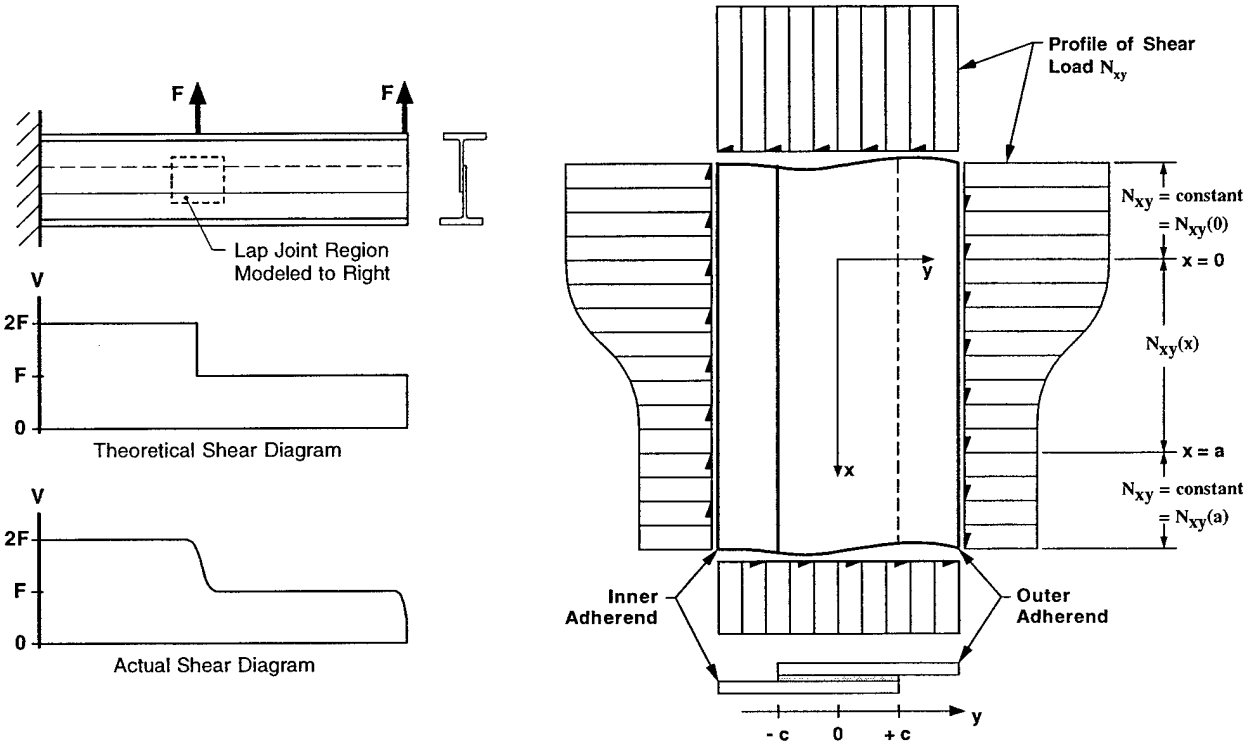

FIGURE 9. LAP-JOINTED SHEAR WEB UNDER SPATIALLY VARYING SHEAR LOAD

This function is valid in the width direction of the joint in the region $0 < x < a$ and is constant in the y direction. For $x < 0$, N_{xy} is constant at 17.5 N/mm and for $x > a$, N_{xy} is constant at 8.75 N/mm. The calculation is performed using the same joint geometry for two laminated composite adherend cases: (1) woven glass/epoxy and (2) unidirectional carbon/epoxy. The geometry of the joint and the material properties of the adherends and adhesive are given in table 1. Both of these symmetrically laminated composite adherends have a ±45°-ply orientation content of 50%, with the remainder of the plies oriented at 0° and 90° in equal proportion (25% each). Furthermore, the thickness and material of both the inner and outer adherends are the same. This condition is a special case where the stiffness of the inner and outer adherends are the same. A joint with matching adherend stiffness is referred to as a balanced joint. Since stiffness is

TABLE 1. SEMI-INFINITE JOINT GEOMETRY AND MATERIAL PROPERTIES

Joint Parameter	Symbol	Value
Length of bond overlap	$2c$	12.7 mm
Joint width over which loading varies	a	25.4 mm
Inner and outer adherend thickness	t_i, t_o	2.54 mm
Adhesive thickness	t_a	0.254 mm
Adhesive shear modulus	G_a	1.1 GPa
Glass/epoxy laminate effective shear modulus (case 1)	G^i_{xy}, G^o_{xy}	6.5 GPa
Glass/epoxy laminate effective tensile modulus (case 1)	E^i_y, E^o_y	17.2 GPa
Carbon/epoxy laminate effective shear modulus (case 2)	G^i_{xy}, G^o_{xy}	21.4 GPa
Carbon/epoxy laminate effective tensile modulus (case 2)	E^i_y, E^o_y	82.7 GPa

computed as the product of modulus and thickness, it is conceivable that a composite joint can be balanced with respect to shear loading but not balanced with respect to tension or compression loading. This is due to the ability to independently tailor tension and shear moduli in a composite through choice of laminate ply angles.

The τ^o_{xy} stress in the outer adherend and the τ^a_{xz} adhesive stress are calculated using the closed-form solution given by equations 9 and 14. These results are compared to a finite difference numerical solution of the governing equation 6. The finite difference model was constructed to represent the outer adherend in the region of the bond overlap and over which the loading varied ($-c < y < c$, $0 < x < a$). The grid spacing was 0.508 mm in the x direction and 0.127 mm in the y direction. The finer spacing in the y direction is necessary to capture the high-stress gradients existing along this direction, particularly at the termination of the joint overlap, at $y = \pm c$.

For the materials and geometry given in table 1, the adherend and adhesive stresses are computed and normalized by a running average shear stress (i.e., average depends on x-position). The average shear stress in the outer adherend can be calculated by recognizing that each adherend carries a proportion of the applied load which is dependent upon the stiffness of the outer adherend relative to the inner.

$$\left(\tau^o_{xy}\right)_{ave} = \frac{G^o_{xy} N_{xy}}{G^o_{xy} t_o + G^i_{xy} t_i} \tag{26}$$

The average inner adherend shear stress can be calculated by replacing G^o_{xy} in the numerator of equation 26 with G^i_{xy}.

The normalized adherend and adhesive shear stress profiles are shown in figures 10 and 11 for both the glass/epoxy and carbon/epoxy adherend cases. In these figures, the closed-form solution is referred to by the abbreviation CF, and the finite difference results by FD. The

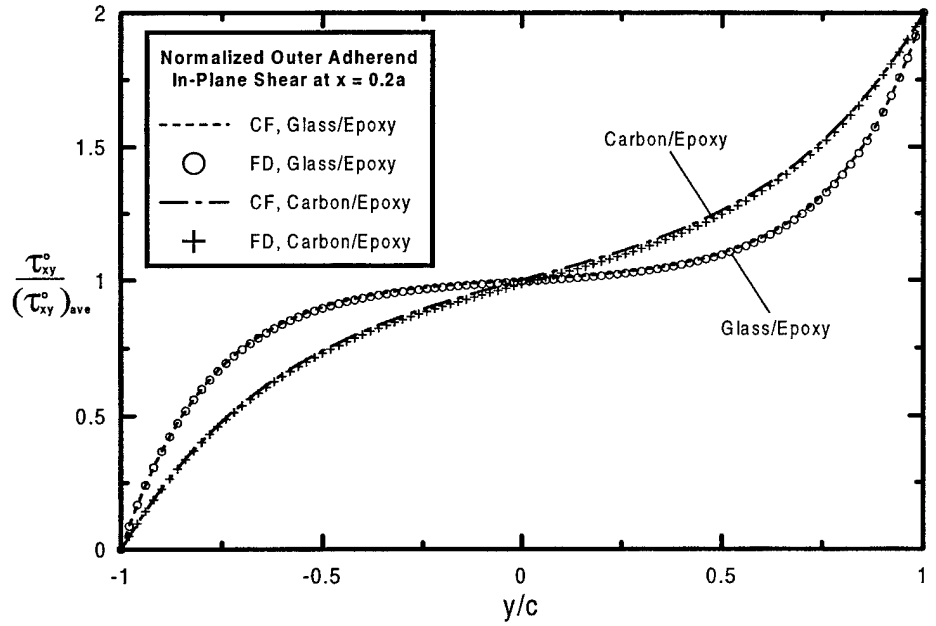

FIGURE 10. τ^o_{xy} ADHEREND IN-PLANE SHEAR STRESS, $\left(\tau^o_{xy}\right)_{ave} = 3.28$ MPa

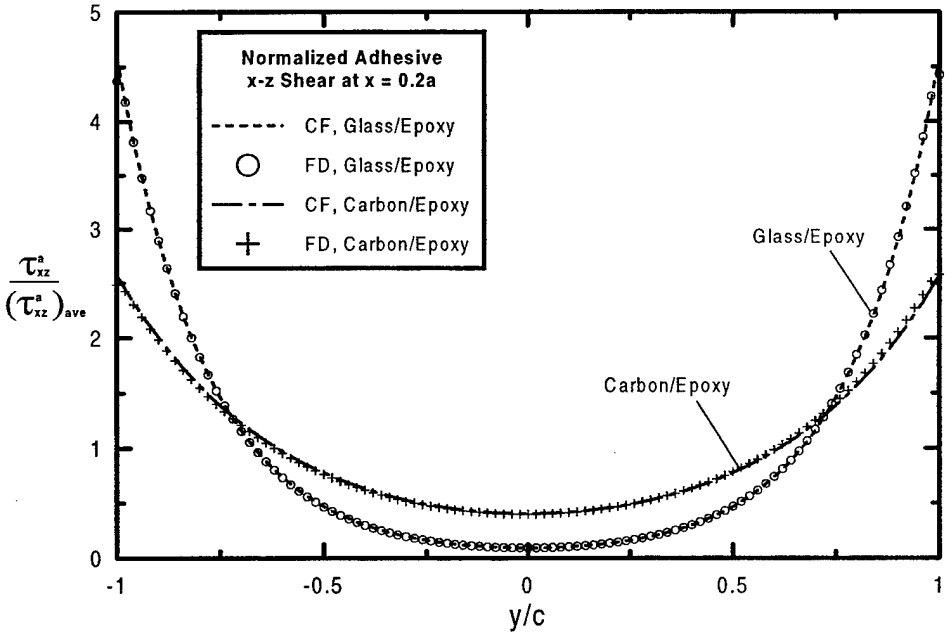

FIGURE 11. τ^a_{xz} ADHESIVE SHEAR STRESS, $\left(\tau^a_{xz}\right)_{ave} = 1.31$ MPa

stresses are plotted along the path $x = 0.2a$, which is a location away from a region of near constant applied loading (e.g., $x = 0$), and for which the loading function is nonlinear in x (i.e., $\partial^2 N_{xy}/\partial x^2 \neq 0$). These criteria were used to select the location for solution comparison in order to demonstrate that the solution developed is valid for any general, smooth, x-varying load function.

Figures 10 and 11 show that the closed-form solution is nearly identical to the finite difference results. Note the different rate of load transfer between the two joint materials. The carbon/epoxy adherend has a significantly higher shear modulus, resulting in a more gradual transfer of shear loading between the two adherends (see figure 10). The shear stress in the inner adherend, τ_{xy}^{i}, can be obtained from equation 1 once the outer adherend stress τ_{xy}^{o} is known. For a balanced joint, the inner adherend shear stress is simply a mirror image of figure 10, about the $y = 0$ axis.

The adhesive shear stress τ_{xz}^{a}, shown in figure 11, is a maximum at the edges of the joint at $y = \pm c$. This figure shows that a joint of identical geometry with more compliant (glass/epoxy) adherends results in significantly higher shear stress peaks. Conversely, a joint with stiffer adherends (carbon/epoxy) carrying the same loads has a higher minimum stress at the center of the overlap and may need to be designed with a greater overlap length so as to maintain a low stress "elastic trough" that is long enough to avoid creep [12] in the adhesive. In joint design, it is necessary to address both the maximum and minimum stress levels in the adhesive, the former to avoid initial (short-term) failures near the joint extremities, the latter to resist viscoelastic strain development under long-term loading. For an unbalanced joint (e.g., t_o = 1.5 mm), one edge of the joint (at $y = +c$) would have a higher value of shear stress than the other side (at $y = -c$).

3.4.2 Validation by Finite Element Analysis.

Further validation of the closed-form solution is demonstrated by comparison of the adhesive shear stress predicted by equation 14 with finite element analysis (FEA) results. Consider the system shown in figure 12. Here a lap-jointed aluminum panel of dimensions, support, and loading configuration shown in the figure produces a region of approximately uniform shear stress resultant N_{xy} away from the free edge. The overlap dimension of the panel is $2c$ = 12.7 mm, the adherends have thickness $t_i = t_o$ = 1.016 mm, and the bondline thickness is t_a = 0.508 mm. The Young's modulus of the aluminum is 68.9 GPa, and the shear modulus of the adhesive is G_a = 1.46 GPa. Also in figure 12 is the FEA mesh used for analysis. Note that solid elements needed to be used in modeling the joint due to the nature of applying shear loading to a lap joint geometry. In contrast, tension-loaded joints can often be analyzed using two-dimensional FEA models.

The applied load F = 623 N was chosen such that a theoretically constant (by simple Strength of Materials calculation) shear flow in the web of 17.5 N/mm exists. The FEA prediction of N_{xy}, plotted in figure 12 as a function of the x and y directions, reveals that the actual average shear flow is 18.7 N/mm, and is approximately constant over the hatched region (see figure 12) away from the free edge. This value of N_{xy} = 18.7 N/mm is used as the loading for the closed-form prediction of adhesive shear stress (equation 14) along the path A-B indicated in figure 12. Figure 13 plots the FEA and closed-form predictions of τ_{xz}^{a} along path A-B. The closed-form solution over-predicts the peak shear stress by less than 2%. It is clear from the comparison shown in figure 13 that the closed-form solution provides an accurate prediction of adhesive shear stress. Additionally, the closed-form equations provided a solution at much less computational cost than FEA. Note that additional refinement of the FEA mesh at the bond

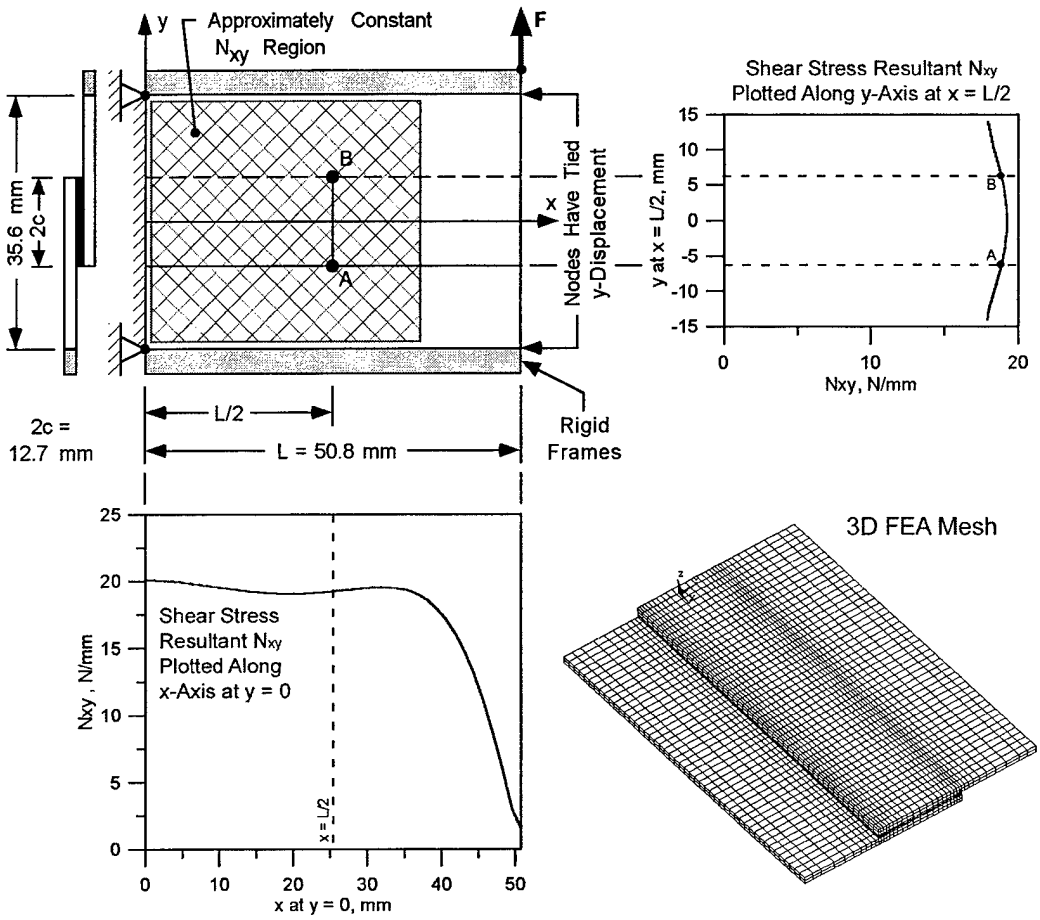

FIGURE 12. SHEAR STRESS RESULTANT PROFILE IN LAP-JOINTED ALUMINUM PANEL

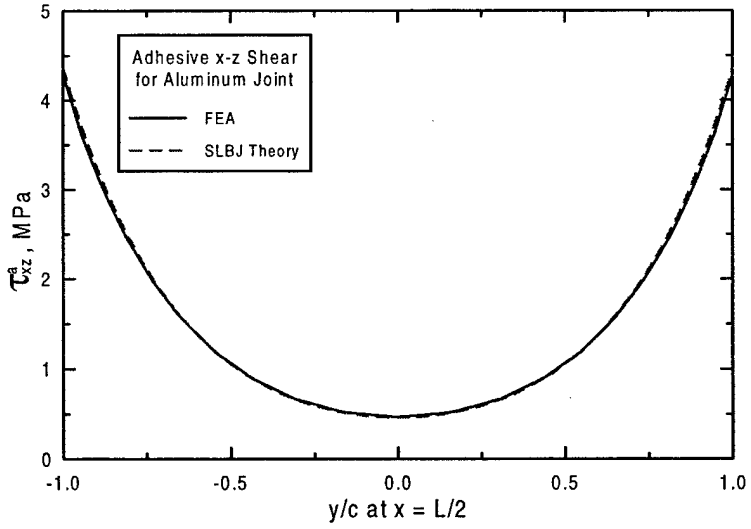

FIGURE 13. COMPARISON OF ADHESIVE SHEAR STRESS PREDICTED BY FEA AND CLOSED-FORM SOLUTION; τ^a_{xz} PLOTTED ALONG PATH A-B IN FIGURE 12

overlap terminations, at $y = \pm c$, would result in a more accurate shear stress distribution in the adhesive at these free edges. The shear stress actually goes to a zero value since these are traction free boundaries. However, since this transition occurs over such a small distance (at length scales equivalent to the bondline thickness), the relatively coarse FEA mesh used in the analysis does not predict this behavior.

3.4.3 Elastic Limit Prediction for Combined Loading.

An I-beam of bonded construction is shown in figure 14. This beam is representative of the wing spar, illustrated in figure 3. Applied pressure loading can produce significant shear in the web of the I-beam. Additionally, for the case of a wing structure, internal fuel pressure and mass reaction loads can produce tension loading in the web, as indicated in figure 14. The stress resultants N_{xy} and N_y associated with these stresses are shown in the figure. In order to validate a safe design, it is desirable to calculate the maximum loads, N_{xy} and N_y, which the joint can carry.

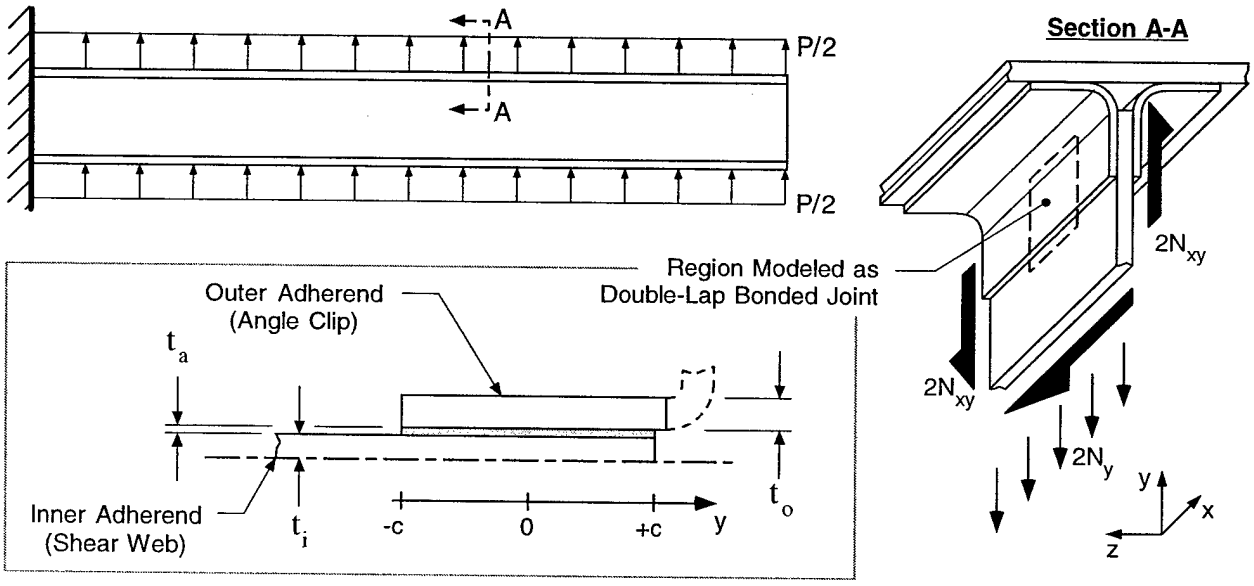

FIGURE 14. BONDED I-BEAM LAP JOINT; LOADS APPLIED THROUGH SHEAR WEB ARE TWICE THE LOADS USED IN JOINT ANALYSIS DUE TO DOUBLE-LAP SYMMETRY

For this design case study, the I-beam shear web and angle clips, shown in figure 14, are constructed of high modulus graphite/epoxy in a balanced and symmetric lay-up with all of the plies oriented in the ±45° directions. A high content of ±45° plies in the shear web is desirable for providing an I-beam with maximum stiffness under transverse loading. For a joint to be balanced (in the joint stiffness sense, as opposed to lamination) under both shear and tension load, the clip should be selected to be of the same material, lay-up, and thickness as half of the web. Table 2 lists the geometry and material properties relevant to analyzing this joint.

TABLE 2. I-BEAM WEB JOINT SPECIFICATIONS

Joint Parameter	Symbol	Value
Web and clip thickness	$t_i = t_{web}/2$, t_o	1.02 mm
Web and clip tensile/compressive modulus	E_y^i, E_y^o	14.5 GPa
Web and clip shear modulus	G_{xy}^i, G_{xy}^o	44.8 GPa
Web and clip tensile/compressive strength	$F_y^{tu} \approx F_y^{cu}$	110 MPa
Web and clip shear strength	F_{xy}^{su}	296 MPa
Adhesive shear modulus	G_a	1.46 GPa
Adhesive shear yield stress	τ^y	37.9 MPa

Profiles of adhesive shear stress arising due to the N_{xy} and N_y loads are plotted in figure 15 using equations 14 and 19 for various overlap lengths. The plots show that as the overlap length gets smaller, the minimum stress (at $y = 0$) increases, and the stress distributions become more uniform. Beyond a certain overlap length, the maximum shear stress in the adhesive asymptotically approaches a constant value, as shown in figure 16. This result is contrary to the stress predicted when assuming an average (uniform) shear stress profile along the joint length. The error of such an assumption is made clear by the plots of average shear stress, in figure 16. Using average shear stress calculations can result in a significantly nonconservative prediction of a joint's performance.

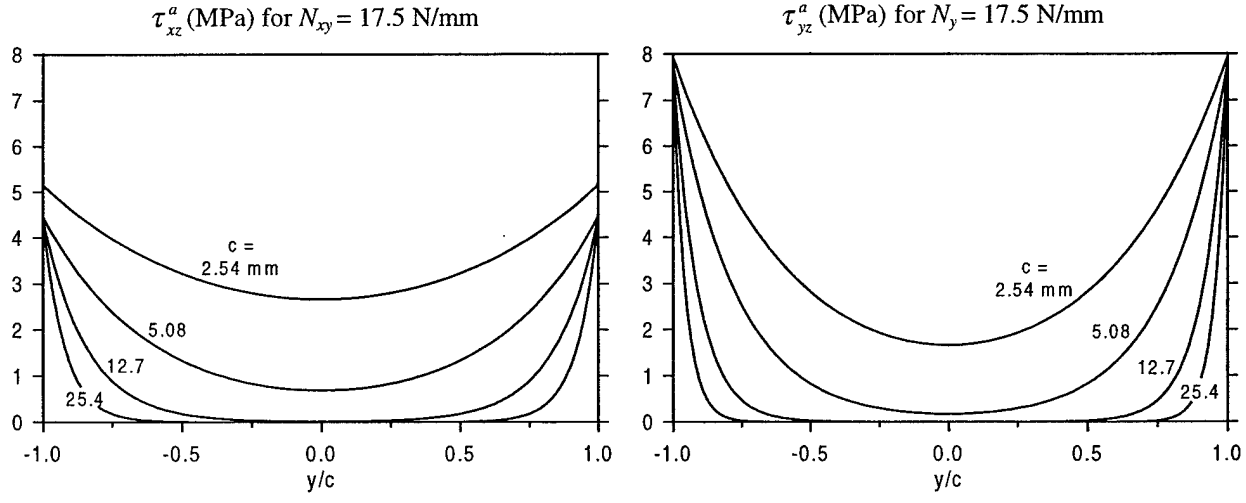

FIGURE 15. ADHESIVE SHEAR STRESS PROFILES FOR t_a = 0.254 mm

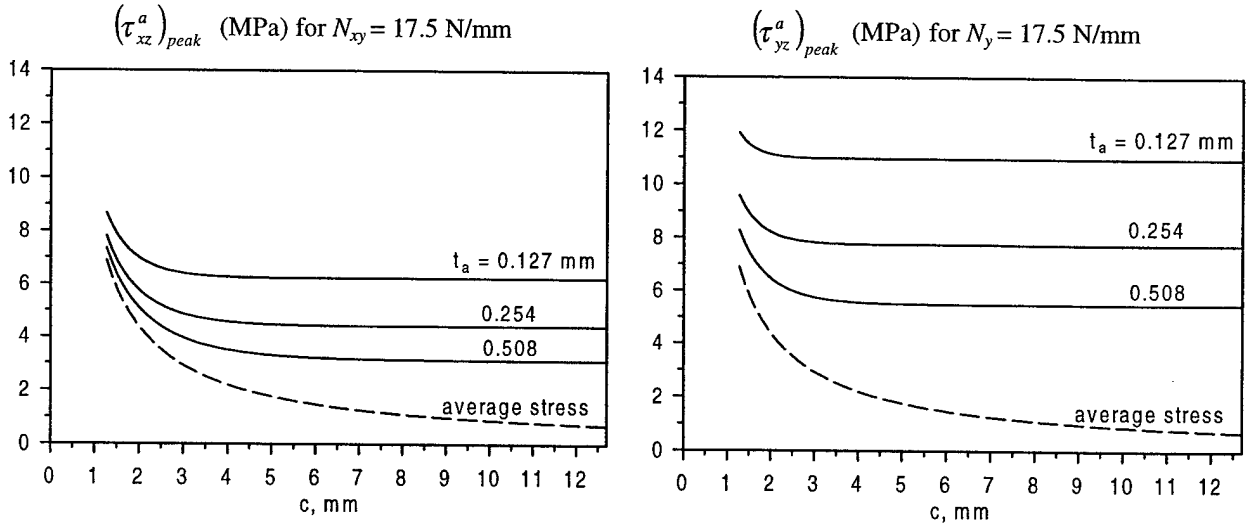

FIGURE 16. PEAK ADHESIVE SHEAR STRESS (AT $y = c$) FOR VARIOUS BOND THICKNESS t_a

The selection of the optimum joint overlap length and thickness depends on the actual load the part must hold, as well as considerations highlighted by Hart-Smith [12] regarding creep of the adhesive. Hart-Smith recommends that the minimum stress in the adhesive remains less than one-tenth of the adhesive yield stress in order to prevent creep. Furthermore, in a design which permits plastic yielding of the adhesive, the presence of a large "elastic trough" is desirable in providing the joint with redundant unstressed material which can accommodate flaws in the bond area, thereby resulting in a damage tolerant joint.

Under simultaneous shear and tensile loads, the adhesive is under a state of biaxial shear stress, τ^a_{xz} and τ^a_{yz}. The von Mises yield criterion, given by equation 24, is one method that can be used to determine the elastic limit of the joint. Using the adhesive shear yield stress τ^y listed in table 2 and inserting expressions for the peak components of adhesive shear stress, (equations 18 and 22), an elliptic equation describing the elastic limit as a function of N_{xy} and N_y is calculated.

$$\left(\frac{N_y\lambda_T}{2tanh\lambda_T c}\right)^2+\left(\frac{N_{xy}\lambda}{2tanh\lambda\ c}\right)^2=\left(\tau^y\right)^2 \tag{27}$$

Elliptical surfaces defining the limit of elastic behavior are plotted in figure 17 using equation 27. The joint is expected to behave elastically for load combinations within and plastically for combinations outside of the envelope. A distinction should be made between elastic limit and joint failure. For an adhesive that develops significant plastic deformation before final failure, the joint can have load carrying capacity beyond that defined by the elastic limit. The extent of this capacity is dependent upon the overall joint parameters.

The effect of bondline thickness on the shape of these surfaces is more significant than overlap length. This latter observation is due to the peak values of adhesive shear stress asymptotically

leveling off for increasing overlap length, as shown in figure 16. Note that the analysis presented in this report assumes a constant shear stress distribution in the adhesive thickness direction (in z direction). It has been shown by Gleich, et al. [13] that this assumption yields only a prediction of the average adhesive shear stress, whereas in reality, a significant through-thickness variation in adhesive shear stress exists for thicker bondlines. The shear and peel stresses at the adhesive-to-adherend interface were shown to be much higher than the average value that is predicted by this and Volkersen's [1] theory. Consequently, when evaluating failure in thick bondline joints, one needs to account for this bondline thickness dependency effect in order to achieve accurate failure predictions.

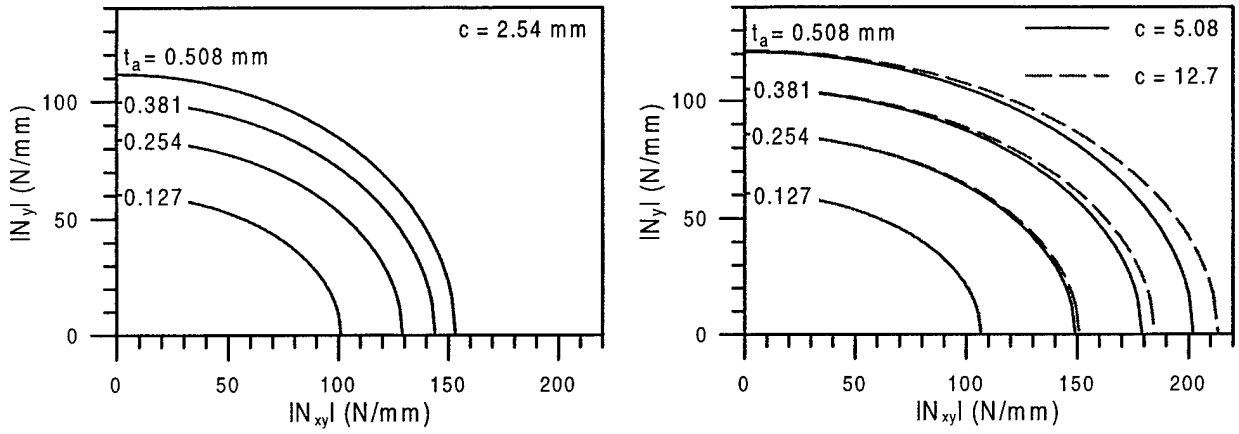

(a) c = 2.54 mm

(b) c = 5.08 and 12.7 mm

FIGURE 17. EFFECT OF BONDLINE THICKNESS AND OVERLAP LENGTH ON ELASTIC LIMIT ENVELOPES FOR COMBINED N_{xy} AND N_y LOADING; PLASTIC BEHAVIOR OCCURS FOR VALUES OF LOAD OUTSIDE OF THE ENVELOPE (ABOVE AND TO THE RIGHT)

The limit curves in figure 17 graphically aid in the design of a shear- and tension-loaded joint. In an overall design, other failure modes to be considered are peel stress (not predicted in the present analysis) in the joint and material failure and buckling of the shear web. For the 1.02 mm thickness ±45° laminates used in this design case study, the failure loads in shear and tension are N_{xy} = 301 and N_y = 112 N/mm, respectively (see table 2 for strengths). These are the upper bounds in N_{xy} and N_y loading that can be applied to the joint due to adherend failure.

In considering the "best" joint design, no singular optimal configuration exists. Factors related to joint fabrication (i.e., 25.4-mm overlap may be easier to construct than 5.02 mm), load carrying capacity requirements, and constraints related to part-to-part assembly must also be considered. Based on the elastic predictions for this example design case study, a desirable configuration is an overlap length of between 12.7 to 25.4 mm (c = 6.35 to 12.7 mm) with a target bond thickness of 0.254 to 0.508 mm. This configuration provides a generous low-stress "trough" that provides the joint with damage tolerance, while at an overlap length that results in the asymptotically approached lowest elastic stress peak.

4. SOLUTION FOR FINITE CASE.

4.1 BONDED DOUBLER.

The previous section treated the case of a semi-infinite joint subjected to a gradient loading. In this section, a closed-form solution of the governing equation 6 is presented for the case of a finite-sized doubler bonded to a base structure that is subjected to remotely applied in-plane shear loading, as shown in figure 18. A doubler is often bonded onto a structure to serve as a reinforced hard point for component attachment, such as an antenna on an aircraft fuselage or to increase thickness at local areas for carrying loads through holes, e.g., a bolted attachment. In this case, the bonded doubler patch can be considered as the outer adherend, and the plate to which it is adhesively joined, the inner adherend. Since the doubler is finite in size along both the x and y axes, a simple solution approach cannot be employed such that the governing equation can be treated as an ordinary differential equation. Here, the full partial differential equation must be solved. The rectangular bonded doubler is a particular configuration for which an assumed τ^o_{xy} stress function can be chosen to satisfy both the boundary conditions of the problem ($\tau^o_{xy} = 0$ at $x = 0, a$ and $y = 0, b$) and the governing equation. A double Fourier sine series satisfies both of these conditions.

$$\tau^o_{xy} = \sum_{m=1}^{\infty}\sum_{n=1}^{\infty} A_{mn} \sin\frac{m\pi x}{a} \sin\frac{n\pi y}{b} \tag{28}$$

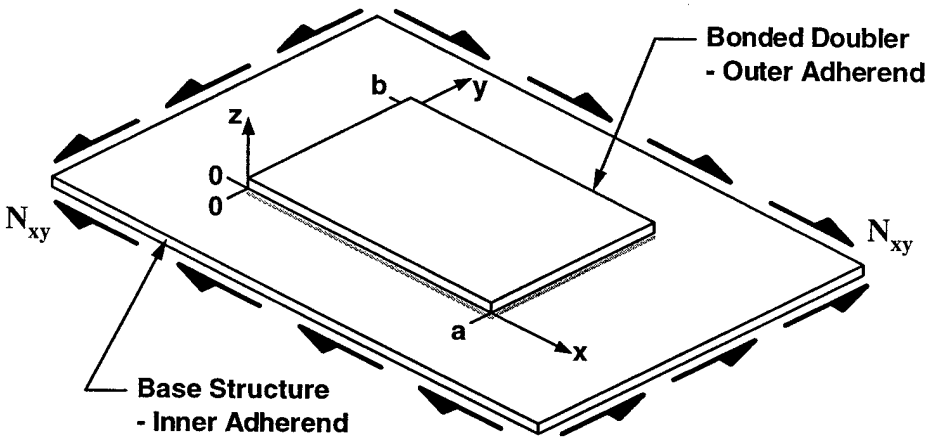

FIGURE 18. FINITE-SIZED DOUBLER BONDED ONTO PLATE WITH REMOTE SHEAR LOADING N_{xy}

The Fourier coefficient A_{mn} is determined such that the governing equation 6 is satisfied. To achieve this, the nonhomogeneous term of the governing equation, C_o, must also be represented by a double Fourier sine series.

$$C_o = \sum_{m=1}^{\infty}\sum_{n=1}^{\infty} C_{mn} \sin\frac{m\pi x}{a} \sin\frac{n\pi y}{b} \tag{29}$$

where C_{mn} is the Fourier coefficient in equation 29 and is calculated by

$$C_{mn} = \frac{4}{ab}\int_0^a\int_o^b C_o(x,y)\sin\frac{m\pi x}{a}\sin\frac{n\pi y}{b}dy\,dx \tag{30}$$

In equation 30, the term $C_o(x,y)$ within the double integral is the nonhomogeneous term of the governing equation 6 and should not to be confused with the C_o on the left-hand side of equation 29. Note that spatially varying $N_{xy}(x,y)$ loading is accounted for through the $C_o(x,y)$ term in equation 30.

Inserting equations 28 and 29 into the governing equation 6, the Fourier coefficient of equation 28 can now be solved for

$$A_{mn} = \frac{C_{mn}}{\left(\frac{\pi m}{a}\right)^2 + \left(\frac{\pi n}{b}\right)^2 + \lambda^2} \tag{31}$$

The series solution given by equation 28 provides the in-plane shear stress distribution within the outer adherend. The adhesive shear stress components, τ_{xz}^a and τ_{yz}^a, are calculated using equations 2 and 3. Note that in the finite-sized joint case, the τ_{yz}^a stress is significant in magnitude at two opposing doubler boundaries $x = 0$ and $x = a$, even for a constant N_{xy} applied load.

4.2 EXAMPLE CALCULATION.

An example calculation is now presented. Consider a thin glass/epoxy structure (inner adherend) carrying shear load. A carbon/epoxy doubler (outer adherend) is bonded to the structure. The geometry of this example problem is listed in table 3. The material properties used in the calculation are taken from table 1. Applied shear load is a constant N_{xy} = 17.5 N/mm.

TABLE 3. FINITE-SIZED DOUBLER GEOMETRY

Doubler Parameter	Symbol	Value
Length of doubler in x direction	a	127 mm
Length of doubler in y direction	b	76.2 mm
Inner adherend thickness; glass/epoxy base structure	t_i	1.27 mm
Outer adherend thickness; carbon/epoxy doubler	t_o	2.54 mm
Adhesive thickness	t_a	0.508 mm

The results of the calculation are shown by the three-dimensional stress surface plots in figures 19 to 21. In figure 19, the doubler in-plane shear stress τ_{xy}^o is plotted. The plots correctly show that this stress goes to zero at the boundaries. Away from the edges, towards the center of the doubler, the stress is the average shear stress, 5.97 MPa, as calculated by equation 26.

The adhesive shear stress component τ^a_{xz}, plotted in figure 20, has maximum magnitude at two opposing edges of the doubler, at $y = 0$ and $y = b$. Similarly, the adhesive shear stress component τ^a_{yz} is maximum at the edges $x = 0$ and $x = a$, as shown in figure 21.

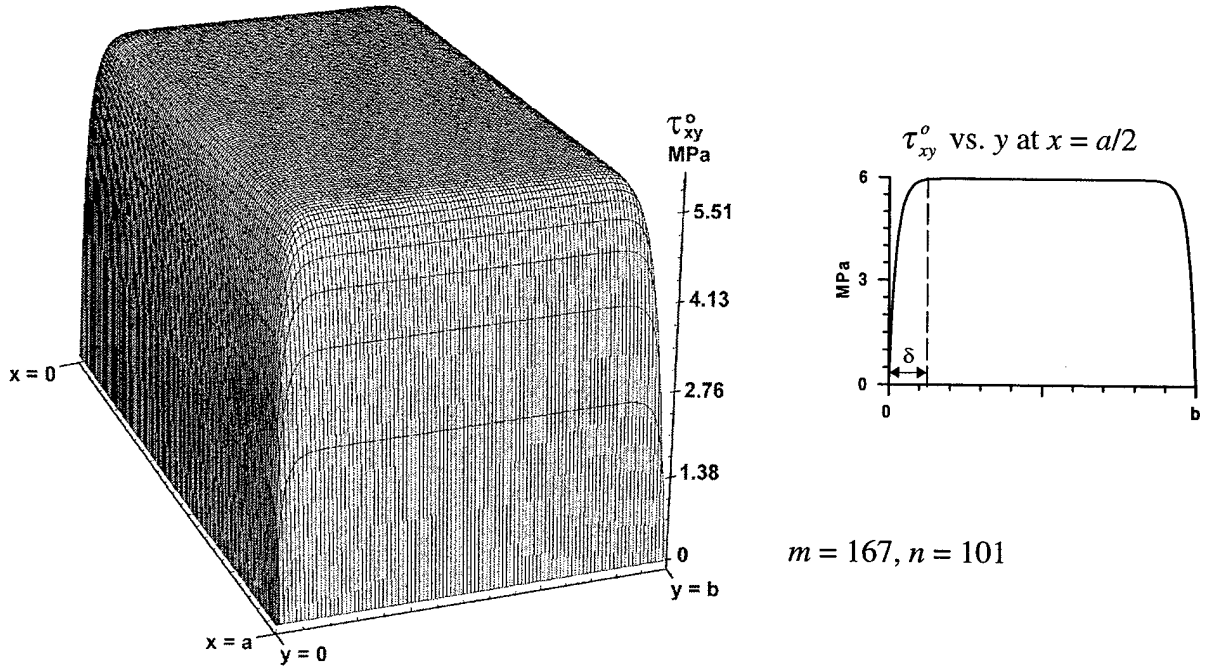

FIGURE 19. SHEAR STRESS τ^o_{xy} IN THE DOUBLER

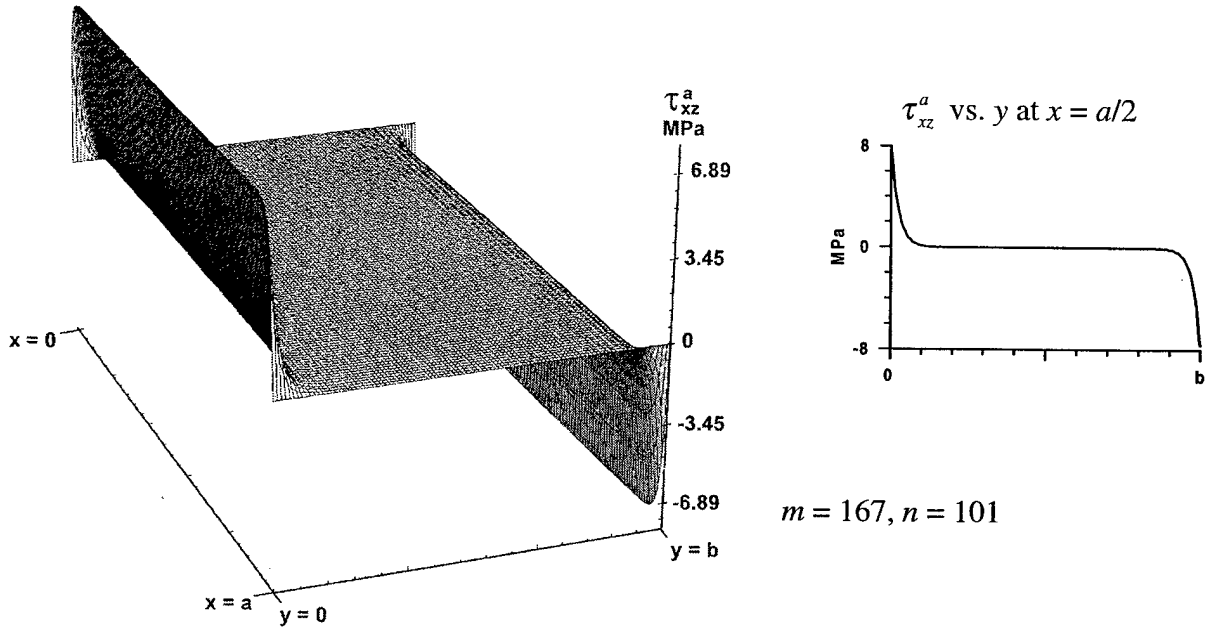

FIGURE 20. ADHESIVE SHEAR STRESS τ^a_{xz}

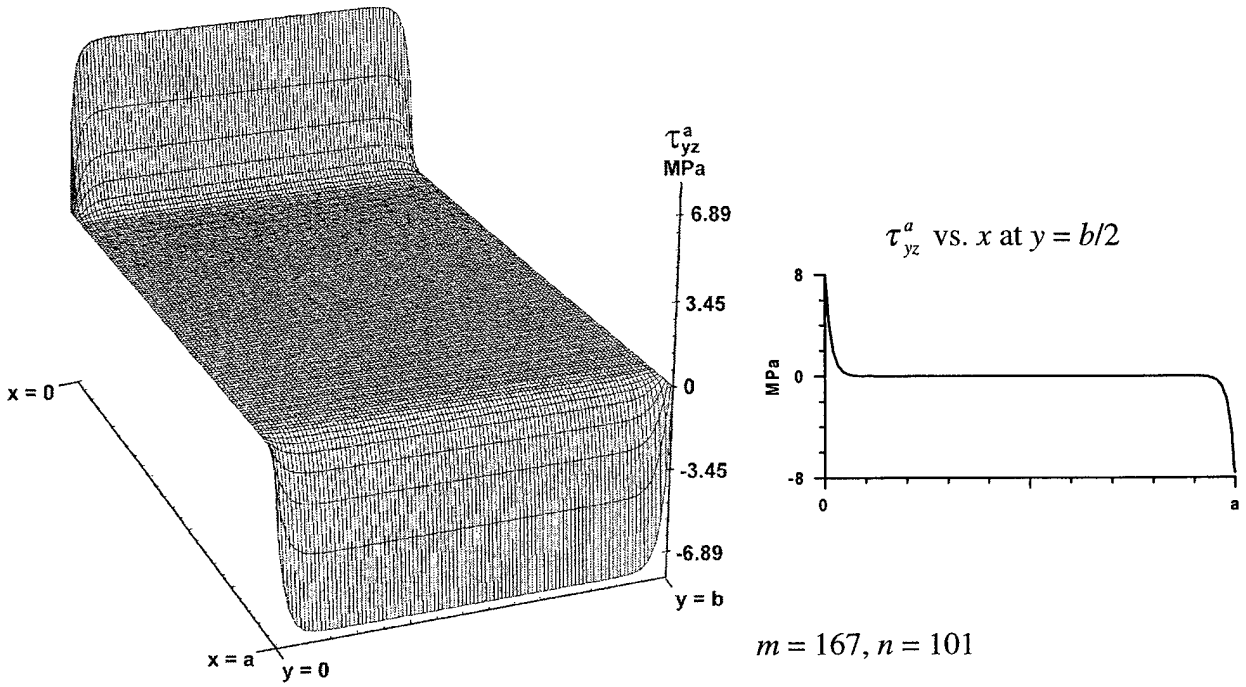

FIGURE 21. ADHESIVE SHEAR STRESS τ^a_{yz}

These plots were generated for a large number of terms (m = 167, n = 101) taken in the series solution, equation 28. A drawback to the sine series solution applied to this problem is that convergence can be slow. This is especially so when the gradients in τ^o_{xy} occur at a length scale that is small compared with the overall size of the doubler, (e.g., less than one-tenth size). Figure 19 shows this to be the case for this example problem. Consequently, a high number of terms in equation 28 need to be used in order to converge upon an accurate solution. Table 4 lists the values of peak adhesive shear stress for combinations of the number of terms taken in the double sine series solution. Values of $(\tau^a_{xz})_{max}$ were taken at the location $x = a/2$, $y = 0$, and $(\tau^a_{yz})_{max}$ values were taken at $x = 0$, $y = b/2$.

TABLE 4. CONVERGENCE OF DOUBLE SINE SERIES SOLUTION (Units are in MPa)

n	41		101		167		501	
m	$(\tau^a_{xz})_{max}$	$(\tau^a_{yz})_{max}$	$(\tau^a_{xz})_{max}$	$(\tau^a_{yz})_{max}$	$(\tau^a_{xz})_{max}$	$(\tau^a_{yz})_{max}$	$(\tau^a_{xz})_{max}$	$(\tau^a_{yz})_{max}$
41	6.74	5.76	7.69	5.75	7.96	5.75	8.24	5.75
101	6.70	7.21	7.65	7.19	7.92	7.19	8.20	7.19
167	6.70	7.66	7.64	7.64	7.90	7.63	8.18	7.63
501	6.70	8.13	7.64	8.10	7.91	8.09	8.19	8.09

The table shows that increasing the number of terms taken in m yields more accuracy in predicting $(\tau^a_{yz})_{max}$, while an increasing number of terms taken in n yields a more accurate prediction of $(\tau^a_{xz})_{max}$. This is due to the number of m and n terms each directly improving the representation of the doubler in-plane shear stress in the x and y directions, respectively, from which $(\tau^a_{yz})_{max}$ and $(\tau^a_{xz})_{max}$ are computed. Obviously a better representation of τ^o_{xy} in the x direction (more m terms) would result in an improved calculation of τ^a_{yz}. Similar statements can be made regarding τ^a_{xz} and the number of n terms. Note that a higher predicted value of $(\tau^a_{yz})_{max}$ is calculated for a combination of m = 501, n = 41 than for m = 501, n = 501. This is due to the nature of the assumed sine series solution which predicts an oscillation of the τ^a_{yz} stress about a mean value when plotted versus y at any station in x (e.g., at x = 0) for a given number of terms taken in m. As shown in figure 22, increasing the number of terms taken in n results in a convergence to that mean value (i.e., higher frequency yields lower amplitude), while changing the number of terms taken in m will change the mean value, as is reflected in table 4. The same arguments apply to explain this apparent loss of accuracy when comparing values of $(\tau^a_{xz})_{max}$ for m = 41, n = 501 with $(\tau^a_{xz})_{max}$ calculated for m = 501, n = 501. Note that these differences, as listed in table 4, are negligible at less than 1% for the number of terms used in constructing this convergence study. However, they would be higher if a lower number of m and n terms were taken, e.g., m = 21 (see figure 22).

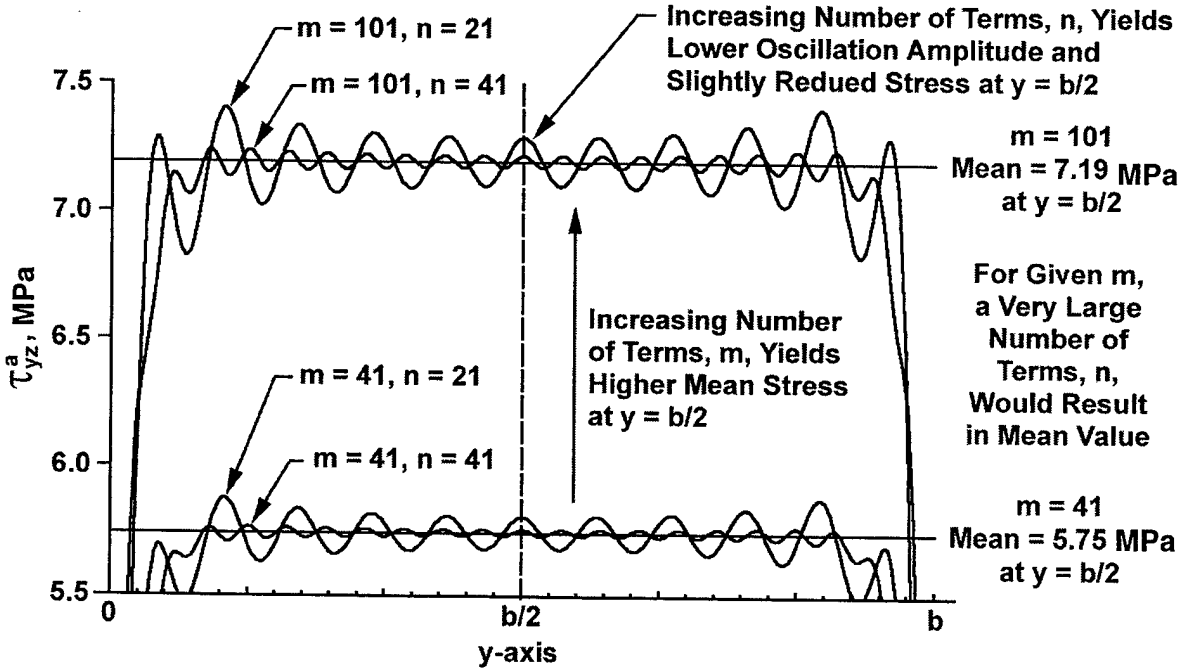

FIGURE 22. OSCILLATORY PROFILE OF ADHESIVE SHEAR STRESS τ^a_{yz} AT x = 0 FOR LOWER NUMBERS OF TERMS m AND n USED IN INFINITE SERIES SOLUTION

The underlined values in table 4 indicate the solution from which the plots in figures 19 to 21 are constructed, i.e., at m = 167, n = 101. These values for m and n were chosen such that roughly ten half-sine waves fit within the edge boundary zone, δ, where gradients in τ^o_{xy} exist. The size of this boundary zone is indicated in figure 19. A calculation of the boundary zone size, δ, can be made using the relationship

$$\delta = -\frac{\ln \varepsilon}{\lambda} \tag{32}$$

where λ is given by equation 7 and ε is an arbitrarily chosen small tolerance value close to zero, e.g., use ε = 0.01. Equation 32 is derived from the general form of the semi-infinite joint solution, which assumes $\tau^o_{xy} \propto e^{-\lambda x}$.

In regions away from the corners of the doubler, the adhesive shear stress profiles for τ^a_{xz} and τ^a_{yz} can be accurately predicted using the semi-infinite joint solution approach presented in the previous section. The validity of performing such a calculation can be verified by observing the τ^a_{xz} adhesive stress profile in figure 20. In the regions away from the two opposing doubler boundaries, x = 0 and x = a, the stress profile τ^a_{xz} is only a function of y. Furthermore, this profile is identical to that which would be predicted by a semi-infinite joint calculation. To compute the $\tau^a_{xz}(y)$ adhesive shear stress profile, away from the edges x = 0 and x = a, the boundary conditions, τ^o_{xy} = 0 at y = 0 and y = b, must be applied to the assumed solution, equation 9, in order to solve for the coefficients A_o and B_o. Equation 2 is then used to compute the adhesive stress component acting in the x-z plane.

$$\tau^a_{xz}(y) = \frac{C_o}{\lambda^2}\left[(\cosh \lambda b - 1)\frac{\sinh \lambda y}{\sinh \lambda b} - \cosh \lambda y + 1\right] \quad \text{for } \delta < x < (a - \delta) \tag{33}$$

Equation 33 can be rewritten for $\tau^a_{yz}(x)$ by replacing y with x, and b with a.

$$\tau^a_{yz}(x) = \frac{C_o}{\lambda^2}\left[(\cosh \lambda a - 1)\frac{\sinh \lambda x}{\sinh \lambda a} - \cosh \lambda x + 1\right] \quad \text{for } \delta < y < (b - \delta) \tag{34}$$

These formulae both predict a peak magnitude of shear stress, $(\tau^a_{xz})_{max} = (\tau^a_{yz})_{max}$ = 8.33 MPa, at the same locations for which values listed in table 4 were obtained. This peak magnitude of adhesive shear stress can be considered the exact value. Comparing this value with the m = 167, n = 101 case in table 4, the values listed there are 8% below the exact. The values of $(\tau^a_{xz})_{max}$ and $(\tau^a_{yz})_{max}$ for the m = 501, n = 501 case are less than 3% below the exact value. A plot of equation 33 for the bonded doubler example is compared in figure 23 with the double sine-series-based stress prediction using equation 28 for the m = 167, n = 101 case.

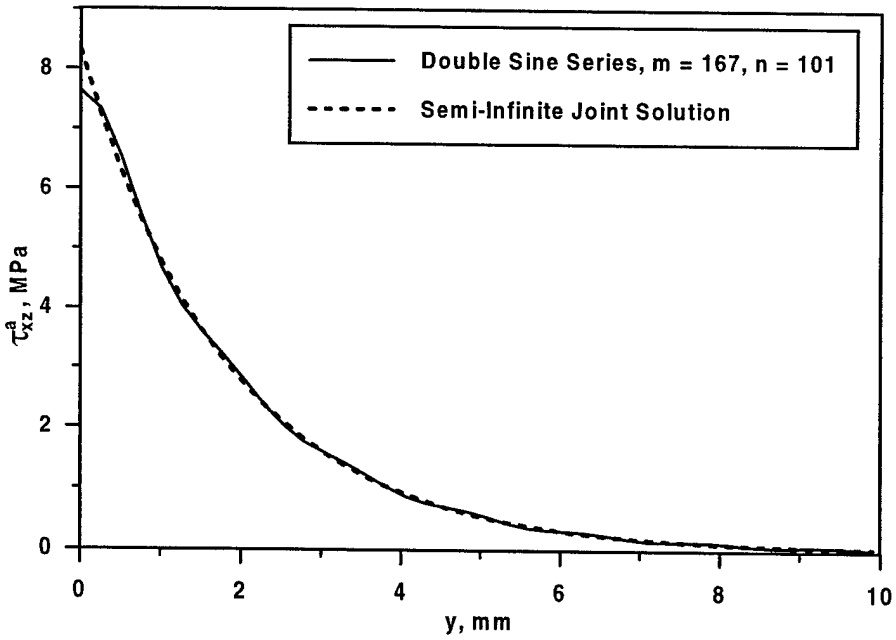

FIGURE 23. COMPARISON OF ADHESIVE SHEAR STRESS τ^a_{xz} AT $x = a/2$ AS PREDICTED BY DOUBLE SINE SERIES AND SEMI-INFINITE JOINT SOLUTIONS

4.3 APPLICATIONS.

The stress τ^o_{xy} in the interior region of the doubler away from the edges is a nominal value calculated by equation 26. For doublers of practical size, this nominal stress region is quite large compared to the boundary zone regions (see figure 19). Consequently, a self-equilibrating applied load, or geometry that perturbs the stress state within the confines of this nominal stress zone, would not affect the prediction of adhesive stresses at the doubler boundary (or visa versa). An example would be an antenna mount, or a hole serving as a bolted attachment point, as shown in figure 24. A crack being repaired using an adhesively bonded patch, shown in figure 25, would also fall under this condition, so long as the crack geometry is smaller than the patch overall dimensions, and the resulting perturbed stress state does not affect the nominal stress state in regions close to the patch boundaries. Note that a separate analysis must be performed to account for the effects of stress concentrations that arise due to the hole or crack geometry. Such a calculation is greatly simplified when it is not necessary to simultaneously account for the boundary stress gradients.

Figures 24 and 25 show biaxial tension loading in addition to applied shear stress resultants. As mentioned previously, the tensile (or compressive) loads can be accounted for by using a tension-loaded, bonded joint analysis and superposing the results of this analysis with the stress states predicted by the applied shear loading.

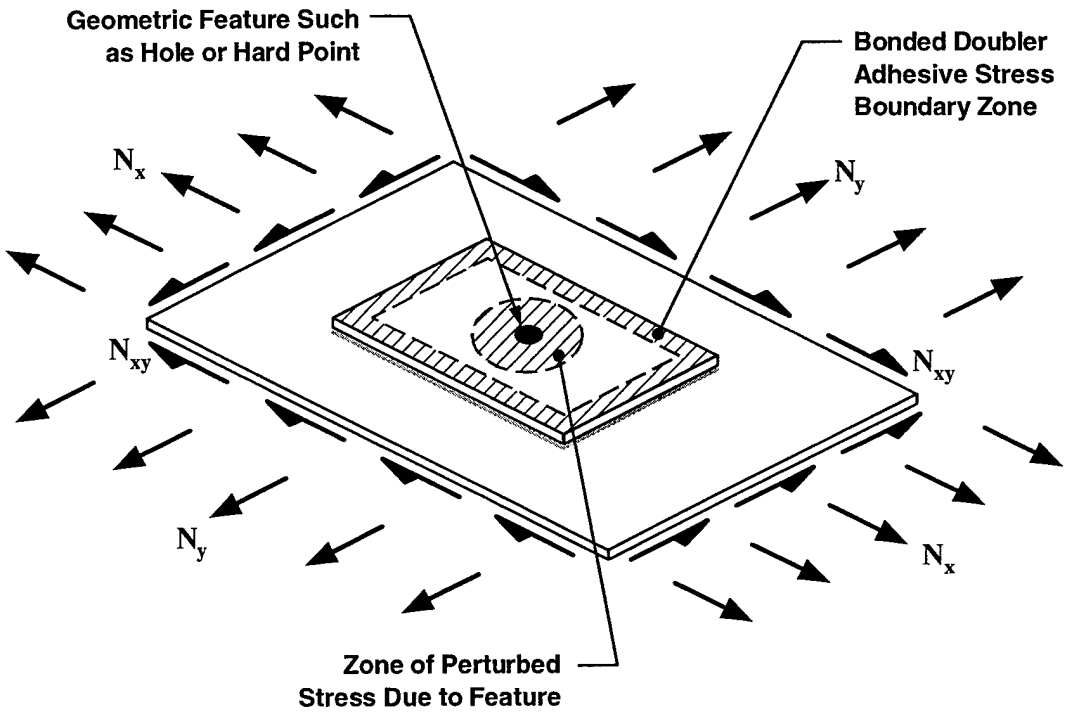

FIGURE 24. BONDED DOUBLER APPLIED TO REINFORCE REGIONS WITH HOLES OR HARD POINTS

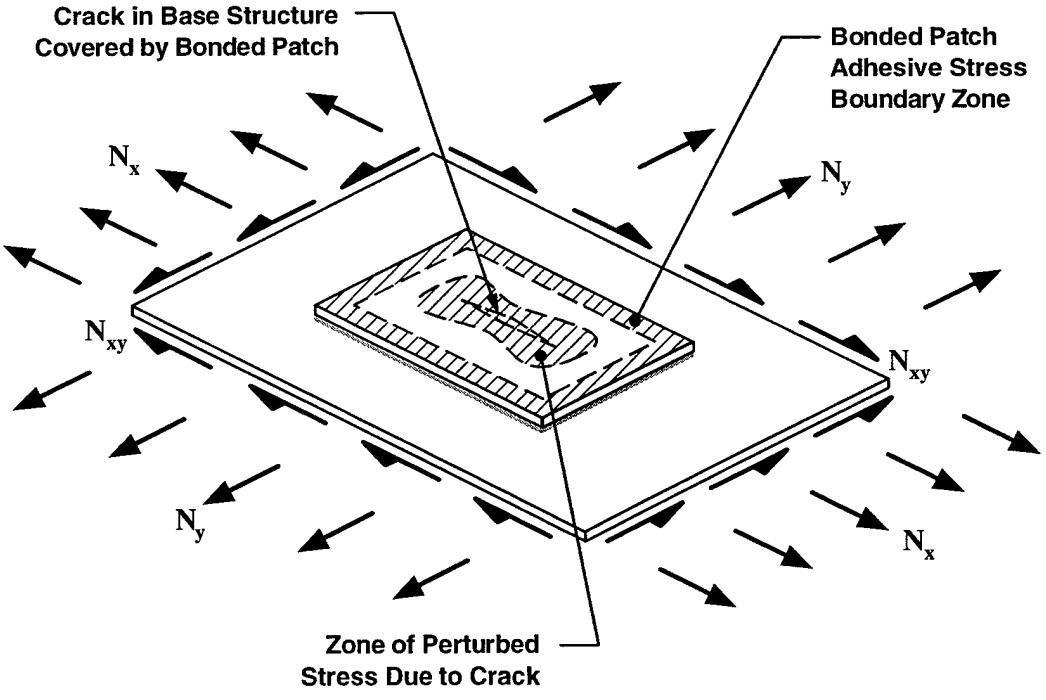

FIGURE 25. CRACK REPAIR USING BONDED PATCH

5. CONCLUSIONS.

A general treatment of an adhesively bonded lap joint, loaded by spatially varying in-plane shear stress resultants, has been presented. The resulting governing partial differential equation describes the in-plane shear stress in one of the adherends. Solution of this equation generally permits the calculation of two adhesive shear stress components, τ_{xz}^{a} and τ_{yz}^{a}. While analogous to the governing equation written for the tension-loaded lap joint case, this equation differs in that it is inherently two-dimensional. Additionally, since the second order derivative terms of the equation can be represented by the Laplacian Operator, ∇^2, the governing equation can be readily applied to solve bonded joint problems which are more suitably described by cylindrical coordinates.

For a semi-infinite joint, a closed-form solution to the governing equation was obtained under the conditions that the applied loading varies smoothly in the direction across the width of the bonded joint (i.e., perpendicular to the overlapping direction). This closed-form solution has been verified to be accurate through comparison to a numerical finite difference solution of the governing differential equation. Additionally, FEA has been used to verify that the solution accurately predicts the stresses in an in-plane shear loaded joint.

The semi-infinite joint solution is directly analogous to the well established solution for a tension-loaded joint. Under simultaneous shear and tension loading, the adhesive stress states predicted by each load case can be linearly superimposed to determine a biaxial shear stress state. One approach to predicting the elastic limit of a joint under a biaxial stress state is to employ the von Mises yield criterion. The result is a user-friendly graphical representation of a structure's elastic operating range that can be used to validate the load carrying capability of a given design (within elastic range). Additionally, since the solutions are in closed form, the effect of geometric and material parameters on joint performance can readily be explored, therefore assisting in the selection of design parameters, as well as aid in the evaluation of how manufacturing tolerances affect joint behavior.

A closed-form solution for a finite-sized bonded doubler was obtained using a double sine series approximation. For this case, both the τ_{xz}^{a} and τ_{yz}^{a} adhesive shear stress components are significant. In order to achieve an accurate sine-series-based solution, the minimum number of terms taken in the series should be such that at least five full sine wave oscillations exist within the length scale over which gradients in the doubler shear stress exists. Alternatively, an approximate, yet accurate, prediction of the maximum values of τ_{xz}^{a} and τ_{yz}^{a} stresses occurring at the boundaries of the doubler can be determined by treating the finite-sized doubler as semi-infinite. While this solution excludes the corner regions of the doubler, the adhesive shear stresses are predicted to be zero at these locations, and thus, the discrepancy of this solution approach is inconsequential.

In the finite-sized doubler example calculation, a boundary zone at the edge of the doubler was shown to exist. This boundary zone is the edge-adjacent region in which gradients in τ_{xy}^{o} are significant, and thus τ_{xz}^{a} and τ_{yz}^{a} are of significant magnitude. The size of this boundary zone is

governed by the term λ, in equation 7. For stiffer adherends or a thicker adhesive layer, the boundary zone would be larger. In the analogous tension-loaded joint case, this λ term would contain the Young's Modulus of the adherends, which, in general, is several times larger (at least for isotropic materials) than the shear modulus. Therefore, the boundary zone would typically be larger for the tension-loaded case than the shear-loaded case. Finally, when numerically modeling the joint, either by finite difference or finite element techniques, knowledge of λ aids in determining what node spacing is adequate enough to accurately resolve gradients in the bond stresses.

In the interior region of the doubler, confined by the boundary zone, the adhesive stresses are null, and the doubler in-plane stress, τ_{xy}^{o}, is a nominal value which depends only on the magnitude of the remote applied loading, N_{xy}, and the relative stiffness of the adherends. Within this nominal stress zone, geometric features can exist (or self-equilibrating loads applied), such as a crack in the base structure (inner adherend) or a hole passing through both adherends. If these features are such that the resulting perturbed stress field surrounding the feature is within the confines of the nominal stress zone, then the two problems of predicting the doubler edge stresses, and the stresses arising due to the geometric feature, can be treated independently. That is, they would not influence each other, thus, greatly simplifying their individual treatment.

The analysis presented is applicable to several joint geometries and applications. There are many geometries for which a closed-form solution is not possible. However, most of these problems can still be solved numerically, since the governing partial differential equation that was derived is well suited for solution techniques based on the finite difference method.

6. REFERENCES.

1. Volkersen, O., "Die Niektraftverteilung in Zugbeanspruchten mit Konstanten Laschenquerschritten," *Luftfahrtforschung*, 15:41-47, 1938.

2. Oplinger, D.W., "Effects of Adherend Deflections in Single Lap Joints," *Int. J. Solids Structures*, 31(18):2565-2587, 1994.

3. Tsai, M.Y., Oplinger, D.W., and Morton, J., "Improved Theoretical Solutions for Adhesive Lap Joints," *Int. J. Solids Structures*, 35(12):1163-1185, 1998.

4. Hart-Smith, L.J., "Adhesive-Bonded Single-Lap Joints," NASA-Langley Contract Report, NASA-CR-112236, 1973.

5. Hart-Smith, L.J., "Adhesive-Bonded Double-Lap Joints, NASA-Langley Contract Report, NASA-CR-112235, 1973.

6. ASTM, "Standard Test Method for Apparent Shear Strength of Single-Lap Joint Adhesively Bonded Metal Specimens by Tension Loading," D1002, 1994.

7. ASTM, "Standard Test Method for Strength Properties of Adhesives in Shear by Tension Loading of Single-Lap Joint Laminated Assemblies," D3165, 1991.

8. Adams, R.D. and Peppiatt, N.A., "Stress Analysis of Adhesive Bonded Tubular Lap Joints," *J. Adhesion*, 10:1-18, 1977.

9. Kim, H. and Kedward, K. T., "Stress Analysis of Adhesive Bonded Joints Under In-Plane Shear Loading," accepted by *J. Adhesion* on October 2000, to be published in 2001.

10. Engineering Sciences Data Unit, "Stress Analysis of Single Lap Bonded Joints," Data Item 92041, 1992.

11. van Rijn, L.P.V.M., "Towards the Fastenerless Composite Design," *Composites Part A*, 27(10):915-920, 1996.

12. Hart-Smith, L.J., "Further Developments in the Design and Analysis of Adhesive-Bonded Structural Joints," in *Joining of Composite Materials, ASTM STP 749*, K. T. Kedward, ed., ASTM, pp. 3-31, 1981.

13. Gleich, D.M., van Tooren, M.J.L., and Beukers, A., "Analysis of Bondline Thickness Effects on Failure Load in Adhesively Bonded Structures," Proceedings of 32nd International SAMPE Technical Conference, November 5-9, 2000, pp. 567-589.